Metal-organic Frameworks Derived Porous Cake-like TiO$_2$ as an Efficient Scattering Layer for Dye-Sensitized Solar Cells

Weiguo Zhang, Shuaishuai Chang, Jiabao Gu, Suwei Yao, Hongzhi Wang[*]

Department of Applied Chemistry, School of Chemical Engineering and Technology, Tianjin University, Tianjin 300350, PR China
[*]E-mail: wanghz@tju.edu.cn

Porous anatase cake-like TiO$_2$ was prepared by annealing Ti-based metal-organic frameworks (MOFs) MIL-125, which was then used as an efficient scattering layer in dye-sensitized solar cells (DSSCs). The morphology and structure of the prepared porous cake-like TiO$_2$ were characterized by SEM, TEM, and XRD. DSSCs with porous cake-like TiO$_2$ as an efficient scattering layer exhibited a photoelectric conversion efficiency (PCE) of 6.91%, which was greater than that of single P25 TiO$_2$ based DSSCs (3.89%). The improved photoelectric conversion efficiency was attributed to the crucial role of porous cake-like TiO$_2$ in promoting surface area and incident light scattering performance, as demonstrated by N$_2$ adsorption/desorption isotherm analysis, diffuse reflectance spectroscopy, incident photon-to-current efficiency (IPCE) analysis, and electrochemical impedance spectroscopy (EIS).

1. INTRODUCTION

Dye-sensitized solar cells (DSSCs), due to their advantages such as low cost, easy fabrication and relatively high efficiency, are now regarded as the best substitutes for traditional silicon solar cells [1]. To enhance the performance of DSSCs, a new system was developed [2-4], several broad absorption spectra dyes were synthesized [5, 6], and new different redox composite electrolytes were prepared [7, 8], from which a highly catalytic activity counter electrode can be established [9, 10]. Specifically, photoanodes undertake remarkably important roles of transporting photogenerated carrier and adsorbing dyes, which ultimately decide the power conversion efficiency of DSSCs to a great extent. Typically, P25 nanocrystalline TiO$_2$ is now the most widely applied photoanode in DSSCs owing to its favorable energy band gaps and excellent capacity of dye absorption. However, P25 nanocrystalline TiO$_2$-based photoanodes also have several disadvantages such as poor surface area, weak interconnectivity, and poor light scattering capability due to poor formation with ineffective

pores, determined by small and regular particle sizes (~25 nm) [11]. To solve these problems, coating large particles onto a P25 nanocrystalline TiO_2 layer to form a double-layered structure is a feasible method. Such a double-layered structure significantly increases the light scattering capability of the photoanode in the DSSCs photoelectric conversion efficiency. Until now, most light scattering materials have focused on anatase TiO_2 particles because of their good electrical conductivity and superior ability in dye adsorption [12-15]. For example, X. Li prepared a hollow box TiO_2 ($BTiO_2$) via a solid-state precursor and used it as a light scattering center, and achieved a high efficiency of 6.1% at the ratio of 20 wt.% [16]. Jung prepared TiO_2 microspheres with a facile solvothermal method, which attained an efficiency of 4.2% [17]. Tanvi embedded appropriately sized mesoporous SiO_2 into a TiO_2 paste at different ratios as recombination inhibitors and efficient light scattering centers. The results indicate that when the ratio of mesoporous SiO_2 reached 0.75 wt%, the power conversion efficiency improved by 50% [18]. Chuen-shii Chou used different average sizes of TiO_2 particles as a light scattering layer to prepare a work electrode for DSSC, and the results show that the performance of DSSC is improved as the average size increased [19] A.M. Bakhshayesh produced a corn-like TiO_2 nanowire that was used as scattering layer for a photoanode, which showed a power conversion efficiency of 7.11%, which is higher than common TiO_2 nanowire because this new morphology can enhance the incident light capture efficiency [20]. Sun Xiaohua reported a special scattering layer consisting of P25 nanoparticles and large rutile particles, and the DSSC based on this photoanode exhibited good light harvesting ability [21]. Zhao Jiahuan investigated the effect of diameter of the scatter center on the performance of DSSC. TiO_2 hollow spheres of different sizes were embedded into TiO_2 nanoparticle films to be used as scattering centers. The study found that the cells exhibits the highest efficiency when the diameter of the scattering center is 600 nm [22].

In our previous work [23], we reported a double-layered DSSC with TiO_2 microspheres employed as an efficient scattering layer, achieving an efficiency of 5.61%. However, all of the approaches mentioned above involve either strict control of the over samples or use of a template, which is unfavorable for large-scale production and increases the fabrication cost of DSSCs. To solve these issues, we must find a novel approach to develop efficient light scattering materials.

Metal-organic frameworks (MOFs), due to their tunable pore structure and large surface area, have attracted much attention in recent years [24-26]. These features of MOFs have enabled them to be widely applied in gas storage/separation [27], catalysis [28], sensor [29], drug delivery [30] and so on. Additionally, applications of MOFs have been extended into energy-related areas, such as lithium-ion batteries [31], supercapacitors [32, 33], solar cells [34], and photocatalytic water splitting [35]. Nevertheless, investigations of MOFs as light harvesting materials for DSSCs are insufficient. For example, Liu converted a leaf-like ZIF film into a porous ZnO nanosheet photoanode, which accelerated the electrolyte diffusion rate, increased dye adsorption, and improved the light harvesting capability. The fabricated DSSC device showed an efficiency of 2.52% [36]. Li prepared hierarchical ZnO from the decomposition of MOF-5, a MOF subclass, and then it used as a scattering layer in DSSCs, achieving an efficiency of 3.67% [37]. Until now, studies based on ZnO photoanodes have hardly achieved a high PCE, which is probably attributed to the unfavorable energy band and low surface area limited by ZnO [11].

Herein, porous anatase cake-like TiO_2 was synthesized via calcination of precursor MIL-125(Ti) and was then used as an efficient scattering layer on top of a P25 nanocrystalline TiO_2 photoanode. The performance of the DSSC with a porous cake-like TiO_2 efficient scattering layer was measured by current density-voltage (*J-V*) curves, incident photon-to-current efficiency (IPCE) and electrochemical impedance spectroscopy (EIS) analyses.

2. EXPERIMENTAL SECTION

2.1. Preparation of porous cake-like TiO$_2$

In this work, MIL-125(Ti) was synthesized according to a previously described preparation method [38, 39]. First, terephthalic acid (2.25 g) was dissolved into anhydrous N,N-Dimethylformamide (DMF, Sinopharm, 99%) (55.6 ml) while magnetically stirred. Then, 5.2 ml methanol (MeOH, Sinopharm, 99%) and 1.45 ml Titanium isopropoxide ($Ti(OiPr)_4$, Aldrich, 95%) were added dropwise. The mixed solution was transferred into a 100 mL Teflon-lined stainless-steel autoclave and was heated at 180℃ for 24 h. The white suspension was centrifuged and washed with MeOH and DMF several times and was dried in a vacuum oven at 80℃ for 12 h. Then, the as-synthesized MIL-125 was heated to 400℃ at a speed of 5℃ min^{-1} and was maintained at that temperature for 6 h under air. After cooling naturally, the resulting white powder product was collected.

2.2. Preparation of photoanodes

First, 4.06 g terpineol and 0.5 g of ethyl cellulose were dispersed in 10 mL ethanol under stirring conditions, and then 1.00 g P25 TiO_2 or the as-prepared porous cake-like TiO_2 was added into the solution and was ultrasonically stirred for 8 h at room temperature until homogeneous. Next, in order to evaporate the ethanol from the mixture, a rotary evaporator was used at 40℃. To fabricate a DSSC with an efficient scattering layer, P25 TiO_2 paste was first spread onto FTO glass using the doctor-blading technique and was sintered at 400°C for 1 h. After chilling to room temperature, porous cake-like TiO_2 as scattering layer was spread on the calcined P25 TiO_2 film according to the same method and was then sintered again at 400°C for 1 h to thoroughly remove organics. After it was naturally cooled, the double-layered photoanode was immersed into a 0.5 mM N719 solution in an airtight and light-free environment for 24 h. As a comparison, a single P25 TiO_2 based photoanode of the same thickness (~10 μm) was prepared and sensitized in the same way.

2.3. DSSC assembly

The cells were assembled in a typical sandwich-type arrangement using the two sensitized photoanodes (active area: 0.2 cm^2) and Pt-coated FTO glass as a counter electrode, respectively named P25-DSSC and DL-DSSC (double-layered DSSC). The electrolyte solution contained 0.1 M LiI, 0.6 M
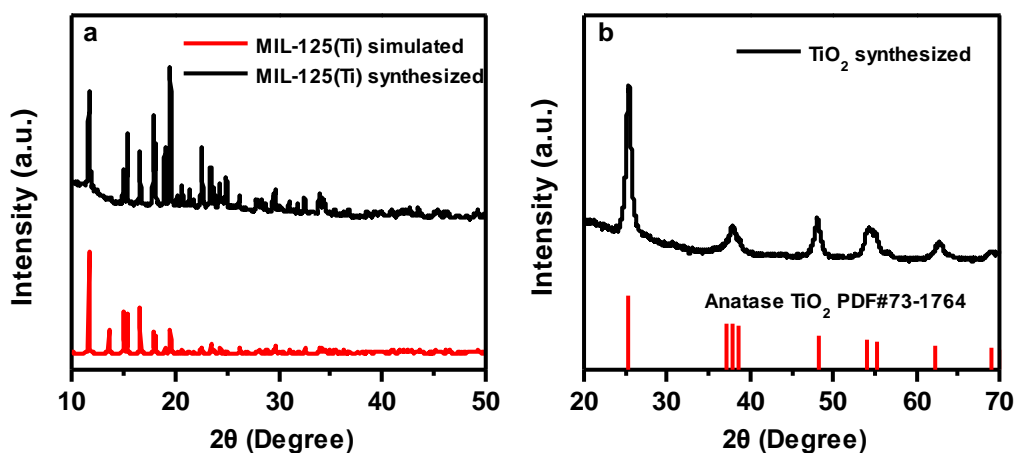
BMII, 0.03 M I_2 and 0.5 M *tert*-butylpyridine (TBP), and the solvent consisted of V(acetonitrile): V(valeronitrile) = (volume ratio: 85:15).

2.4. Characterization

X-ray diffraction (XRD) (Model Bruker D-8 Cu Kα (λ = 1.5406 Å), 40 kV and 100 mA) was used to identified the phase composition of the as-prepared porous TiO_2. Raman spectroscopy used a helium-neon laser at room temperature. N_2 adsorption-desorption isotherms of samples were measured using a Belsorp-Mini instrument (BEL, Inc, Japan) at a constant temperature of 77 K. Specific surface area was calculated via the multipoints Brunauer-Emmert-Teller (BET) method ranging from 0.05~0.3 P/P_0 and the pore size distributions of samples were analyzed using the Barrett-Joyner-Halenda (BJH) method. The morphology and size of precursor MIL-125(Ti) and porous cake-like TiO_2 were determined by transmission electron microscopy (TEM) (JEM 2100F JEOL, Japan) and field-emission scanning electron microscopy (FE-SEM) (Model S-4800, Hitachi Co., Japan). UV–*vis* diffused reflectance spectra of the two photoanodes were collected with a spectrophotometer (TU-1901, PERSEE, China). Photocurrent–photovoltage curves (*J–V* curves) were measured using a CHI 660B electrochemical workstation (Shanghai, China) under simulated sunlight AM 1.5 radiation (100 mW cm^{-2}). Electrochemical impedance spectra (EIS) of DSSCs were measured in the dark with a forward bias of -0.70 V.

3. RESULTS AND DISCUSSION

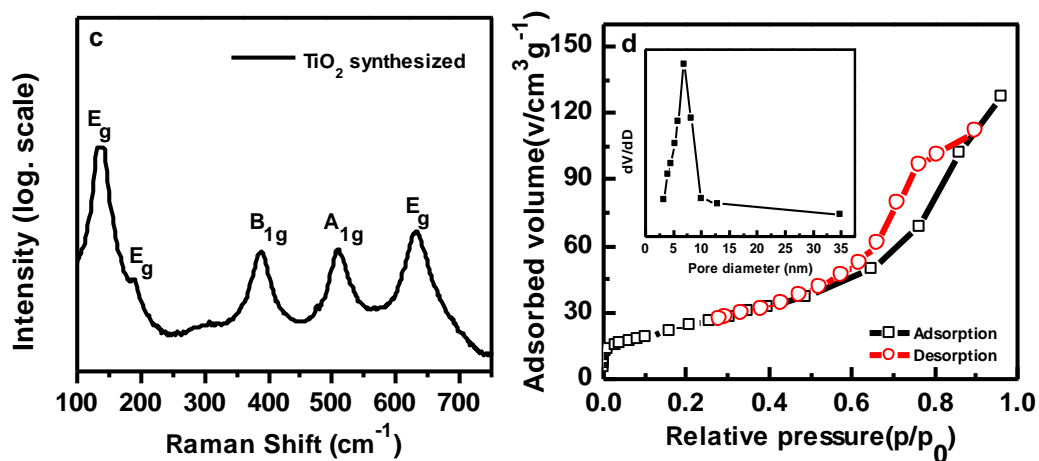## 3.1 Characterization of porous cake-like TiO₂

Figure 1. XRD patterns of synthesized MIL-125 (a) and porous TiO₂ (b), Raman spectra of prepared porous TiO₂(c), Nitrogen adsorption–desorption isotherms and the corresponding pore size distribution curves (inset) of the porous TiO₂ (d)
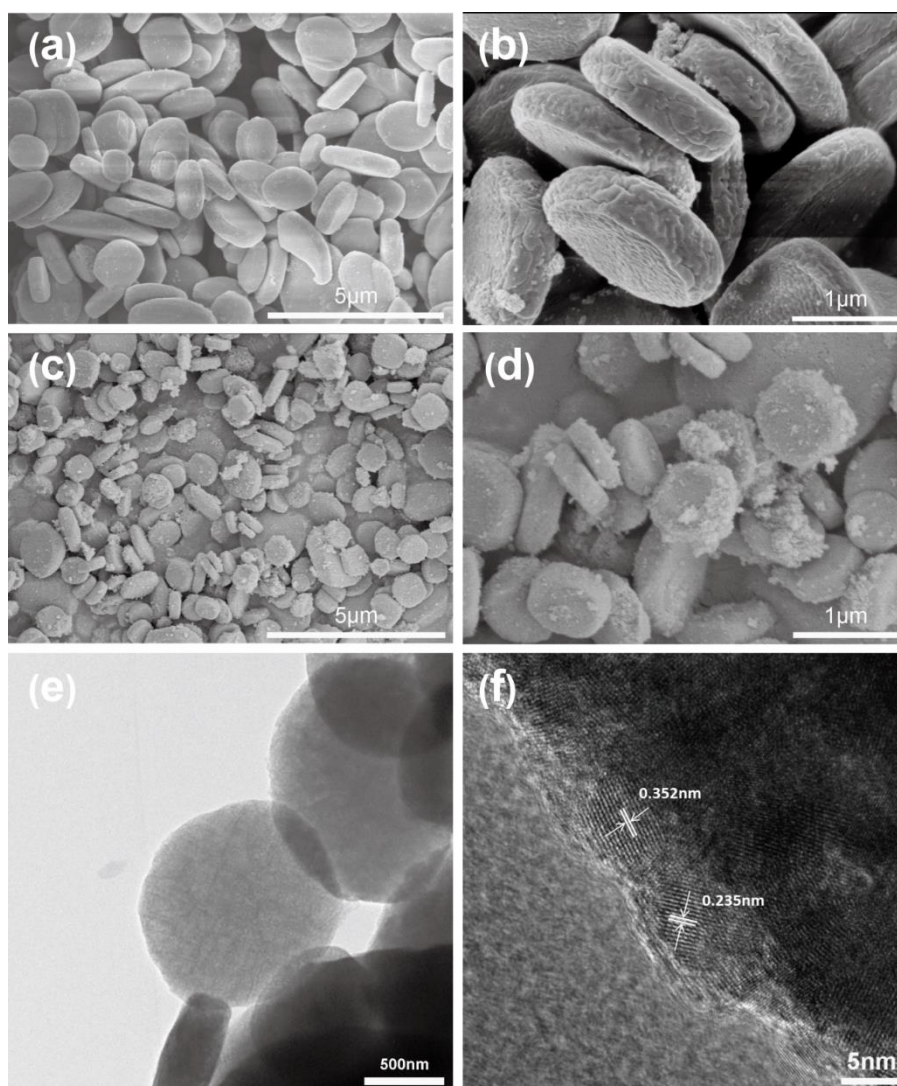

Figure 2. SEM images of synthesized MIL-125 (a and b), porous TiO₂ (c and d), TEM (e) and HRTEM (f) images of porous cake-like TiO₂.

XRD spectra of the MIL-125 precursor before and after the sample was calcined are shown in Fig. 1a and Fig. 1b, respectively. Fig. 1a presents the XRD pattern of the prepared MIL-125, which is consistent with previous results [31, 40, 41]. The peaks at 25.3°, 37.8°, 48.1°, 55.2°, and 62.3°in the pattern of Fig. 1b are indexed to the (101), (004), (200), (211), and (213) planes of typical anatase TiO_2 (JCPDS No. 73-1764), and no additional phases were observed. Fig. 1c displays the Raman spectrum of the synthesized TiO_2, which contains one sharp peak at 149 cm^{-1} and three weak peaks at 400, 515, and 638 cm^{-1}, corresponding to a typical anatase TiO_2 phase [42].

The nitrogen adsorption-desorption isotherm is shown in Fig. 1d, from which the specific surface area of prepared porous TiO_2 and pore size distribution can be directly observed. Results show that the as-prepared porous TiO_2 shows a specific surface area of 125.7 m^2 g^{-1}. The pore diameter distribution results that are inserted in Fig. 1d show that the prepared porous TiO_2 has a mean pore size of ca. 8.2 nm. Thus, it is speculated that when used as a light scattering layer, the prepared porous cake-like TiO_2 will provide efficient transport pathways for electrolyte molecules [43, 44].

SEM images of the synthesized MIL-125 (Fig. 2a, b) reveal cake-like particles with an average diameter of approximately 1.5 μm and thickness of 400 nm. Fig. 2c and its corresponding magnified image (Fig. 2d) show images of the porous anatase TiO_2 derived from MIL-125. From these two pictures, it is apparent that the morphology of the porous cake-like TiO_2 did not change after sintering, but its average diameter and thickness respectively decreased to 0.8 μm and 200 nm. Further investigations of the porous cake-like TiO_2 are illustrated in TEM (Fig. 2e) and HRTEM (Fig. 2f) images. The lattice widths in Fig. 2f are 0.352 nm and 0.235 nm, which are consistent with the basal spacing of (101) and (001) planes of anatase TiO_2 [45, 46].

3.2 Characterization of photoanodes

Many factors can influence the performance of DSSCs, the most important of which is the light scattering capability of the scattering layer [22, 47, 48]. To verify whither or not the porous, cake-like TiO_2 layer increases the light scattering capability, diffuse reflectance spectra of the single P25 and double-layered photoanodes were measured. As shown in Fig. 3a, the single P25 film-based phototanode shows a lower scattering effect in the visible light area (400-700 nm), whereas the photoanode with the light scattering layer shows much stronger reflectance. This can be ascribed to the introduction of the porous cake-like TiO_2 with a special cake-like structure and large particle size, which can provide many more scattering centers and a longer light traveling distance, thus enhancing the scattering effect [19].

The transmittance spectra of this two films are shown in Fig. 3b. The results show that as the wavelength increases, the transmittance of transmitted light increases. Obviously, in the long wavelength area (>550 nm), the single P25 film exhibits higher transmittance than the DL-film. This result can be ascribed to the weak light scattering capability of the P25 nanoparticles. However, when porous cake-like TiO_2 was used as the light scattering layer, its superior light scattering capability given by its special cake-like structure and large particle size will greatly enhance the light scattering

effects inside the double-layered film. Thus, the relatively weak transmittance of the double-layer film was observed, which is very beneficial for light harvesting [22].

Fig. 3c is a schematic diagram of the light path in the double-layer film. As shown in Fig. 3c, porous cake-like TiO2 used as a scattering layer will lengthen the incident light pathway, because of its superior light scattering capability. Thus, it will enhance the light capture probability of dye molecule, increasing the light utilization efficiency and photocurrent. In contrast, for a single P25-based photoanode, more incident light may be lost due to poorer light scattering capability, resulting in a lower photocurrent.
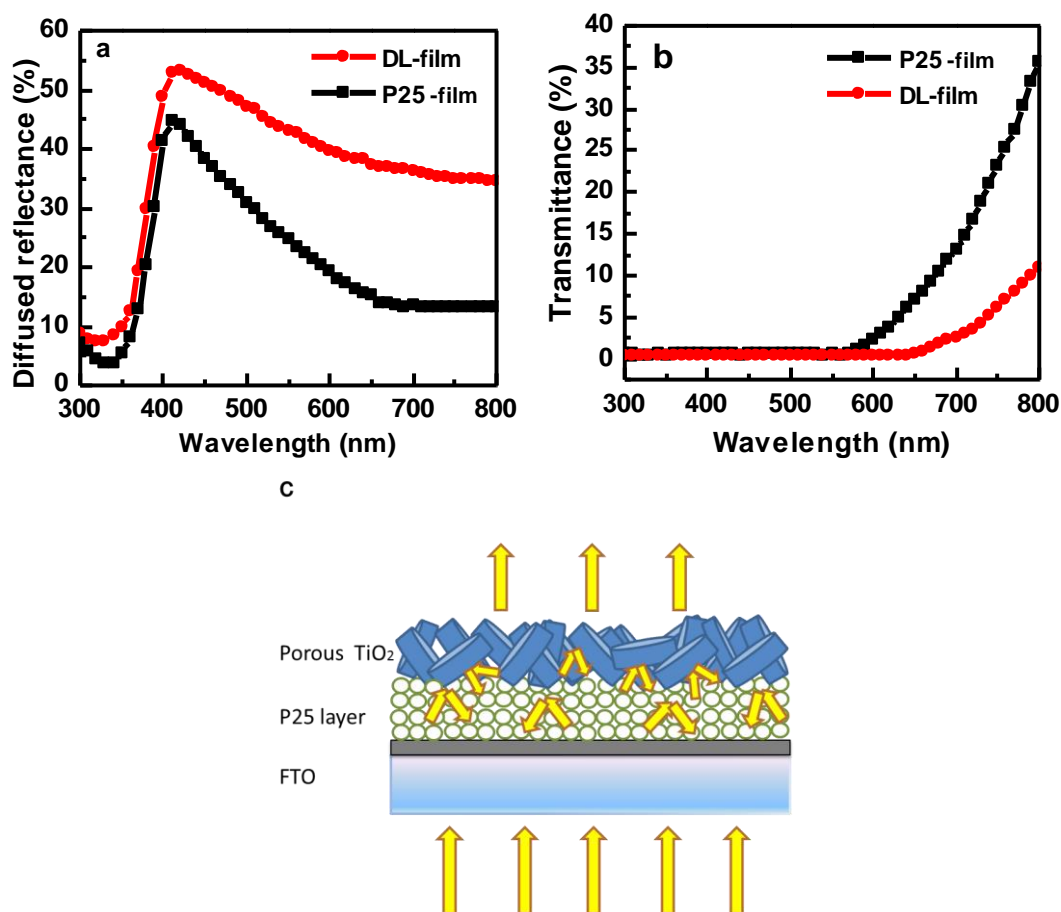

Figure 3. Diffused reflectance spectra (a) and transmission spectra (b) of the single P25-film and double layered film (DL-film). Sketch of light transmission in double-layer film-based photoanode (c).

3.3 Photovoltaic performances of DSSCs

The photovoltaic properties of two the DSSCs were further investigated. Fig. 4a shows the photocurrent-voltage (*J-V*) curves of P25-DSSCs and DL-DSSC. The values of the short-circuit current density (J_{sc}), open-circuit voltage (V_{oc}), fill-factor (*FF*), and photovoltaic conversion efficiency (η) obtained from the *J-V* curves are listed in Table 1. *J*sc and η of DL-DSSC are 15.37 mA/cm^2 and 6.91%, respectively. These are much higher than the corresponding values of P25-DSSC. It is

speculated that the boost in J_{sc} mainly comes from the light scattering effect of the porous cake-like TiO_2 used in the double-layered structure [49]. The porous cake-like TiO_2 lengthens the light traveling distance and thus enhances the probability of photons to be captured by the dye, resulting in remarkable improvements in the photocurrent and photovoltaic conversion efficiency.

DL-DSSC also shows a slightly higher V_{oc} than the single P25, which can be ascribed to the double-layered structure exhibiting a lower electron recombination probability and more efficient charge-transfer process, which causes a positive shift in the Fermi level [50, 51]. The electrochemical impedance spectroscopies (EIS) shown in Fig. 4c prove the results correctly.
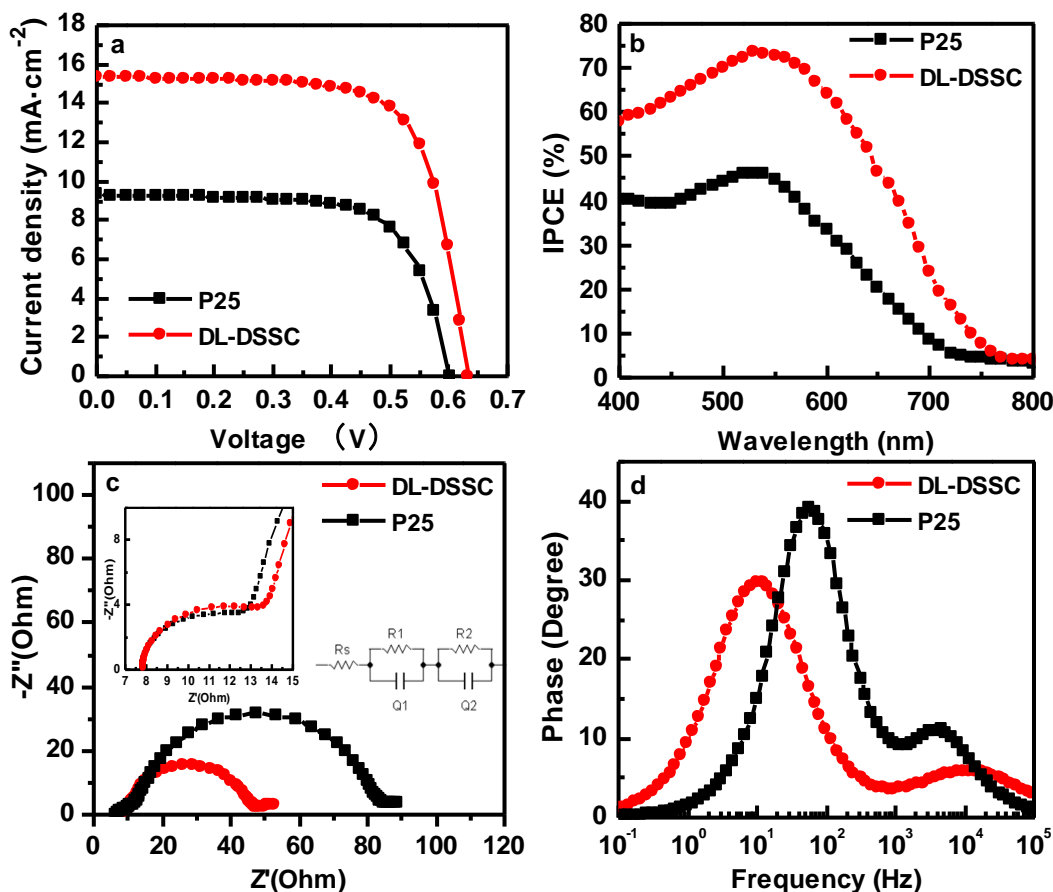

Figure 4. *J-V* curves (a), IPCE spectra (b), Nyquist plots (c), and Bode phase plots (d) of the DSSCs based on the single P25 and double-layered photoanode (DL-DSSC). The inset in (c) is the equivalent circuit used for fit the impedance data.

Table 1. Performance of DSSCs with Various Photoanodes

Sample	J_{sc}(mA·cm^{-2})	V_{oc}(V)	FF	η (%)
P25 DSSC	9.34	0.60	0.69	3.89
DL-DSSC	15.37	0.63	0.71	6.91

Fig. 4b shows the incident photoelectric conversion efficiency (IPCE) spectrum of DSSCs assembled by the single P25 and double-layered photoanodes, measured in the range of 400-800 nm. Due to N719 dye absorption, the maximum values of the two curves appear at approximately 530 nm. The IPCE mainly depends on the light harvesting efficiency (LHE) and the electron collection efficiency. As shown in Fig. 4b, the double-layered photoanode has a much higher IPCE value than that of the single P25 photoanode, which is consistent with the results of *J-V* measurements. The increased IPCE value can be explained as follows. DL-DSSC had a much stronger light scattering capability when the porous cake-like TiO_2 was employed as a light scattering layer in the double-layered DSSC. In addition, the double-layered photoanode exhibits a much slower charge recombination process and increased electron transport properties, resulting in higher electron collection efficiency.

Fig. 4c shows electrochemical impedance spectra (EIS) of the two cells. To fit the series resistance (R_s) and charge-transfer resistance (R_1 and R_2), an equivalent circuit is given in the inset in Fig. 4c. In addition, detailed electrochemical impedance spectra at high frequency are also provided in the insert in Fig. 4c. Resistance (R_s) is mainly related to the resistance of the FTO glass substrate, contact resistance, counter electrode material and the resistance of external circuits. The semicircle in the high-frequency region (R_1) is ascribed to the charge transfer resistance of the electrolyte/counter electrode interface [20]. The semicircle in the intermediate frequency region (R_2) corresponds to charge transfer at the TiO_2/dye/electrolyte interface. The results of EIS analyses are listed in Table 2. This shows that the R_s and R_1 of the two electrodes show no significant difference, but the values of R_2 corresponding to the P25 and double-layered photoanodes are 72.9 Ω and 34.6 Ω, respectively. The smaller value in resistance between these two photoanodes demonstrates that the charge-transfer process at the interface of the photoanode/electrolyte is more efficient and that the electron recombination process in the double-layered DSSC is slower. These results can be explained as follows: the efficient charge-transfer process is due to the close packing of grains that arises from crystal intergrowth within the porous cake-like TiO_2, resulting in the superior interior contacts [52]. The slower electron recombination is related to the 3D structure in porous cake-like TiO_2, given by the MOF (MIL-125) precursor, which facilitates electron transport.

Table 2. EIS parameters of the DSSCs with Various Photoanodes

Sample	$R_s(\Omega)$	$R_1(\Omega)$	$R_2(\Omega)$	f_{max}(HZ)	τ_{eff}(ms)
P25 DSSC	7.9	5.2	72.9	57.4	2.8
DL-DSSC	7.8	5.7	34.6	9.77	16.3

Bode phase plots of the two cells are illustrated in Fig. 4d. The maximum phase peak frequency (f_{max}) was related to the electron transfer and recombination kinetics at the TiO_2/dye/electrolyte interface [53, 54]. Electron lifetime (τ_{eff}) can be expressed as follows [55].

$$\tau_{eff} = 1/(2\pi f_{max})$$

The electron lifetime observed for DL-DSSC (16.8 ms) is longer than that of P25-DSSC (2.7ms), which certifies the lower recombination process and faster electron transfer in DL-DSSC, resulting in a significant improvement in power conversion efficiency [56].

4. CONCLUSION

In summary, MOF-derived porous cake-like TiO_2 was easily prepared via the calcination of MIL-125(Ti) in air, and was used as an efficient scattering layer in a DSSC photoanode. DSSCs made of double-layered photoanodes show a higher efficiency of 6.91% than a single P25-based photoanode, which can be ascribed to enhanced light scattering capability, faster electron transport, and a lower recombination process. This study provides a novel example for applications of MOFs as light scattering materials in DSSC photoanodes, which can be considered as a new strategy to improve DSSC power conversion efficiency.

References

1. B.O'Regan, M. Grätzel, *Nature*, 353 (1991) 737.
2. Y. Lijun, L. Wallace Woon-Fong, *Adv. Mater.*, 25 (2013) 1792.
3. G. Kawamura, H. Ohmi, W.K. Tan, Z. Lockman and H. Muto, A. Matsuda, *Nanoscale. Res. Lett.*, 10 (2015) 1.
4. D. Jiang, Y. Hao, R. Shen, S. Ghazarian, A. Ramos amd F. Zhou, *Applied Materials & Interfaces.*, 5 (2013) 11906.
5. X. Wei, P. Bo, J. Chen, M. Liang and F. Cai, *J. Phys. Chem. C*, 112 (2008) 874.
6. Q.U. Sanyin, W.U. Wenjun, J. Hua, K. Cong, Y. Long and H.E. Tian, *J. Phys. Chem. C*, 114 (2010) 1343.
7. J. Wu, S. Hao, Z. Lan, J. Lin, M. Huang, Y. Huang, P. Li, S. Yin and T. Sato, *J. Am. Chem. Soc.*, 130 (2008) 11568.
8. S. Lee, Y. Jeon, Y. Lim, M.A. Hossain, S. Lee, Y. Cho, H. Ju and W. Kim, *Electrochim. Acta.*, 107 (2013) 675.
9. F. Gong, H. Wang, X. Xu, G. Zhou and Z.S. Wang, *J. Am. Chem. Soc.*, 134 (2012) 10953.
10. W. Hong, Y. Xu, G. Lu, C. Li and G. Shi, *Electrochem. Commun.*, 10 (2008) 1555.
11. W.S. Chi, D.K. Roh, C.S. Lee and J.H. Kim, *J. Mater. Chem. A*, 3 (2015) 21599.
12. A. Hagfeldt, G. Boschloo, L. Sun, L. Kloo and H. Pettersson, *J. Photochem. Photobiol., C Photochemistry Reviews*, 4 (2003) 145.
13. C. Magne, F. Dufour, F. Labat, G. Lancel, O. Durupthy, S. Cassaignon and T. Pauporté, *J. Photochem. Photobiol., A Chem.*, 232 (2012) 22.
14. Y. Kusumawati, M. Hosni, M.A. Martoprawiro, S. Cassaignon and T. Pauporté, *J. Phys. Chem .C*, 118 (2016) 23459.

15. A.G. Thomas, K.L. Syres, *Cheminform.*, 43 (2012) 4207.
16. H. Xiong, L. Xin, M. Zhu, *J. Power. Sources*, 333 (2016) 10.
17. H.G. Jung, S. Nagarajan, S.K. Yong and Y.K. Sun, *Electrochim. Acta,*. 89 (2013) 848.
18. Tanvi, A. Mahajan, R.K. Bedi, S. Kumar, V. Saxena and D.K. Aswal, *Chem. Phys. Lett.*, 658 (2016) 276.
19. C. Chou, M. Guo, K. Liu and Y. Chen, *Appl. Energy*, 92 (2012) 224.
20. A.M. Bakhshayesh, M.R. Mohammadi, H. Dadar and D.J. Fray, *Electrochim. Acta*, 90 (2013) 302.
21. X. Sun, X. Zhou, Y. Xu, P. Sun, N. Huang and Y. Sun, *Appl. Surf. Sci.*, 337 (2015) 188.
22. J. Zhao, Y. Yang, C. Cui, H. Hu, Y. Zhang, J. Xu, B. Lu, L. Xu, J. Pan and W. Tang, *J. Alloys Compd.*, 663 (2016) 211.
23. W. Zhang, J. Gu, S. Yao and H. Wang, *J. Mater. Sci.- Mater. Electro.*, 29 (2018) 7356.
24. L.J. Murray, M. Dincă and J.R. Long, *Chem. Soc. Rev.*, 38 (2009) 1294.
25. T. Pham, K.A. Forrest, P. Nugent, Y. Belmabkhout, R. Luebke, M. Eddaoudi, M.J. Zaworotko and B. Space, *J. Phys. Chem. C*, 117 (2013) 9340.
26. J. Zhang, A.V. Biradar, S. Pramanik, T.J. Emge, T. Asefa and L. Jing, *Cheminform.*, 48 (2012) 6541.
27. O.K. Farha, A.Ö. Yazaydın, I. Eryazici, C.D. Malliakas, B.G. Hauser, M.G. Kanatzidis, S.T. Nguyen, R.Q. Snurr and J.T. Hupp, *Nat. Chem.*, 2 (2010) 944.
28. D. Dang, P. Wu, C. He, Z. Xie and C. Duan, *J. Am. Chem. Soc.*, 132 (2010) 14321.
29. L.E. Kreno, K. Leong, O.K. Farha, M. Allendorf, R.P. Van Duyne and J.T. Hupp, *Chem. Rev.*, 112 (2011) 1105.
30. P. Horcajada, T. Chalati, C. Serre, B. Gillet, C. Sebrie, T. Baati, J.F. Eubank, D. Heurtaux, P. Clayette and C. Kreuz, *Nat. Mater.*, 9 (2010) 172.
31. Z. Wang, X. Li, H. Xu, Y. Yang, Y. Cui, H. Pan, Z. Wang, B. Chen and G. Qian, *J. Mater. Chem. A*, 2 (2014) 12571.
32. B. Liu, H. Shioyama, H. Jiang, X. Zhang and Q. Xu, *Carbon*, 48 (2010) 456.
33. J. Yang, P. Xiong, C. Zheng, H. Qiu and M. Wei, *J. Mater. Chem A*, 2 (2014) 16640.
34. Y. Li, C. Chen, X. Sun, J. Dou and M. Wei, *Chemsuschem.*, 7 (2015) 2469.
35. K. Meyer, M. Ranocchiari and J.A.V. Bokhoven, *Energ. Environ. Sci.*, 8 (2015) 1923.
36. L. Qi, Z.X. Low, F. Yi, S. Leong, Z. Zhong, J. Yao, K. Hapgood and H. Wang, *Microporous Mesoporous Mater.*, 194 (2014) 1.
37. Y. Li, Z. Che, X. Sun, J. Dou and M. Wei, *Chem. Commun.*, 50 (2014) 9769.
38. S. Kim, J. Kim, H. Kim, H. Cho and W. Ahn*, Catal. Today*, 204 (2013) 85.
39. H. Li, Z. Zhang, X. Huang, T. Lan and M. Wei, T. Ma, *J. Energy. Chem.*, 26 (2017) 667.
40. M. Dan-Hardi, C. Serre, T. Frot, L. Rozes, G. Maurin, C. Sanchez and G. Ferey, *J. Am. Chem. Soc.*, 131 (2009) 10857.
41. J. Dou, Y. Li, F. Xie, X. Ding and M. Wei, *Cryst. Growth. Des.*, 16 (2015) 121.
42. S. Balaji, Y. Djaoued and J. Robichaud, *J. Raman. Spectrosc.*, 37 (2010) 1416.
43. J. Yu, J. Fan and C. Bei, *J Power Sources*, 196 (2011) 7891.
44. J. Yu, J. Fan an K. Lv, *Nanoscale*, 2 (2010) 2144.
45. Y. Liu, Y. Cheng, K. Chen, G. Yang, Z. Peng, Q. Bao, R. Wang and C. Wen, *Electrochim. Acta*, 146 (2014) 838.
46. J.D. Peng, C.M. Tseng, R. Vittal and K.C. Ho, *Nano. Energy*, 22 (2016) 136.
47. T. Marimuthu, N. Anandhan, *Mater. Res. Bull.*, 95 (2017) 616.
48. Y. Rui, L. Wang, J.Zhao, H. Wang, Y. Li, Q. Zhang and J. Xu, *Appl. Surf. Sci.*,369 (2016) 170.
49. T. P. Chou, Q. Zhang, B. Russo, G.E. Fryxell and G. Gao, *J. Phys. Chem. C*, 111 (2007) 6296.
50. D. Zhao, T. Peng, L. Lu, P. Cai, P. Jiang and Z. Bian, *J. Phys. Chem C*, 112 (2008) 8486.
51. R. Gao, Z. Liang, J. Tian, Q. Zhang, L. Wang and G. Cao, *Nano. Energy*, 2 (2013) 40.
52. K. Yan, Y. Qiu, C. Wei, Z. Min and S. Yang, *Energ. Environ. Sci.*, 4 (2011) 2168.
53. H. Xu, X. Tao, D.T. Wang, Y.Z. Zheng and J.F. Chen, *Electrochim. Acta*, 55 (2010) 2280.

54. N. Fuke, A. Fukui, R. Komiya, A. Islam, Y. Chiba, M. Yanagida, R. Yamanaka and L. Han, *Chem. Mater.,* 20 (2008) 4974.
55. J. Zhao, Y. Zheng, X. Lu, J.Chen, X. Tao and W. Zhou, *Chem. Phys*., 14 (2013) 1977.
56. P.J. Cameron, L.M. Peter, *J. Phys. Chem. B*, 107 (2003) 14394.